

Supplementary Materials for **A general printing approach for scalable growth of perovskite single-crystal films**

Zhenkun Gu, Zhandong Huang, Chang Li, Mingzhu Li, Yanlin Song

Published 29 June 2018, *Sci. Adv.* **4**, eaat2390 (2018)

DOI: 10.1126/sciadv.aat2390

This PDF file includes:

- fig. S1. The SEM images of the as-grown perovskite single-crystal film.
- fig. S2. Optical microscopy image and AFM image of the perovskite single-crystal film.
- fig. S3. Synchrotron-radiated single-crystal XRD analysis.
- fig. S4. EDS mappings of the perovskite single-crystal films.
- fig. S5. Powder XRD patterns of the perovskite single-crystal films.
- fig. S6. Optical microscopy images of the seed crystal regions.
- fig. S7. Scalable fabrication of perovskite single-crystal films.
- fig. S8. Perovskite single-crystal film growth process.
- fig. S9. The height profiles of perovskite single-crystal films with different thicknesses.
- fig. S10. Responsivity as a function of incident light intensity.

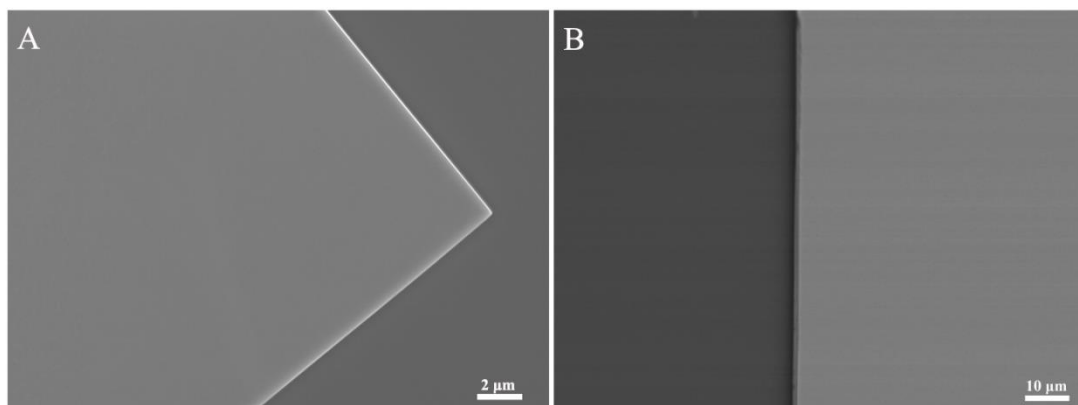


fig. S1. The SEM images of the as-grown perovskite single-crystal film. (A) The film surface. (B) The film profile.

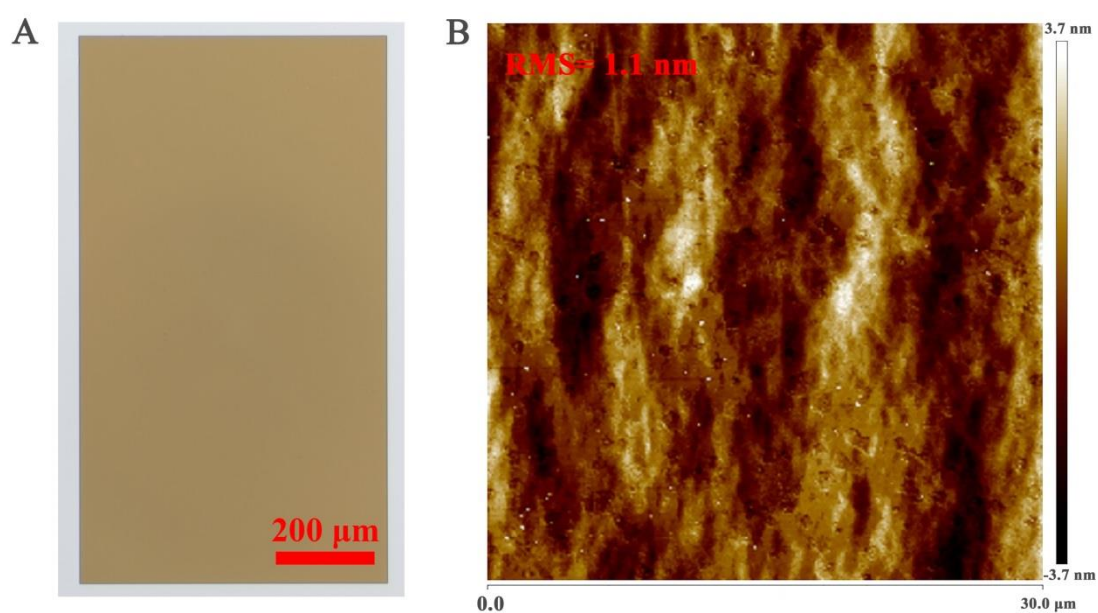


fig. S2. Optical microscopy image and AFM image of the perovskite single-crystal film. (A) Optical microscopy image of millimeter-sized perovskite single-crystal films. (B) AFM image of the as-grown perovskite single-crystal film with the area 30×30 μm.

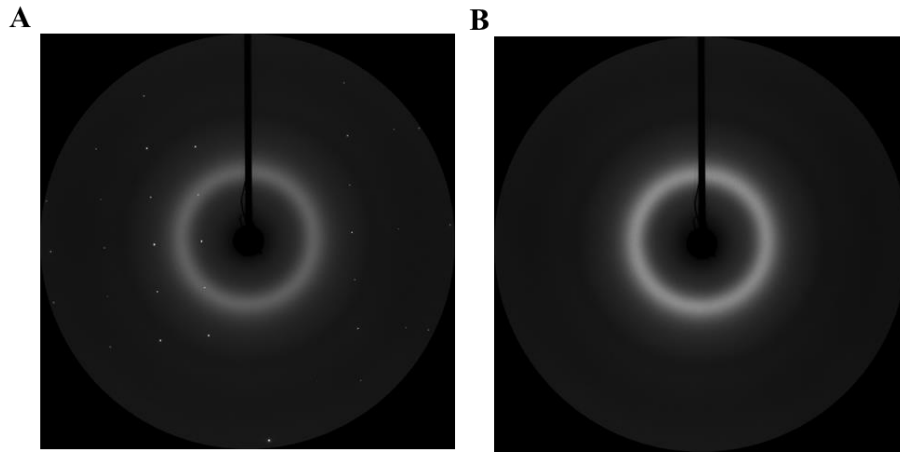


fig. S3. Synchrotron-radiated single-crystal XRD analysis. (A) Synchrotron-radiated single-crystal X-ray diffraction photograph of the perovskite film on quartz glass collected by rotating the incident X-ray beam of $\pm 22.5^\circ$. (B) Synchrotron-radiated single-crystal X-ray diffraction of the blank quartz glass.

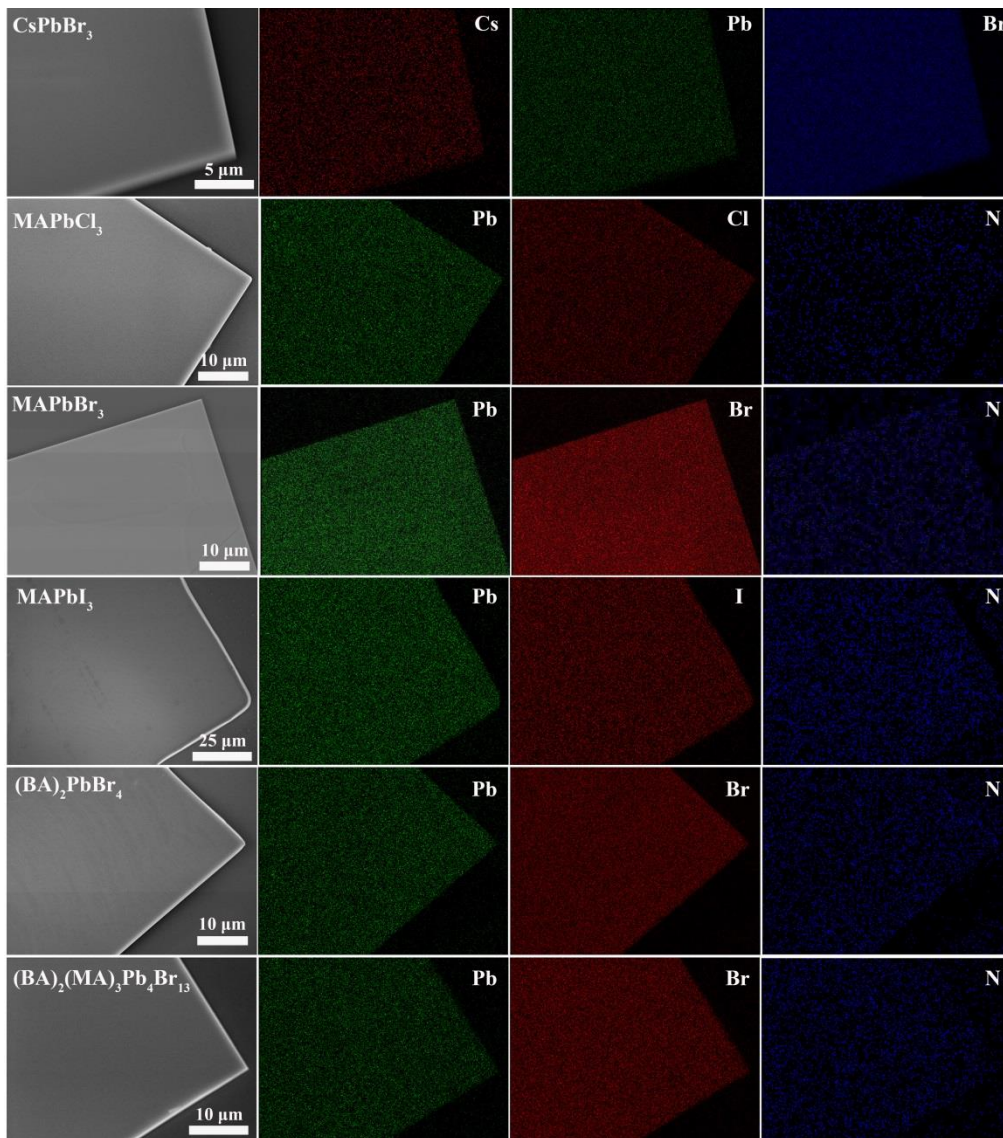


fig. S4. EDS mappings of the perovskite single-crystal films.

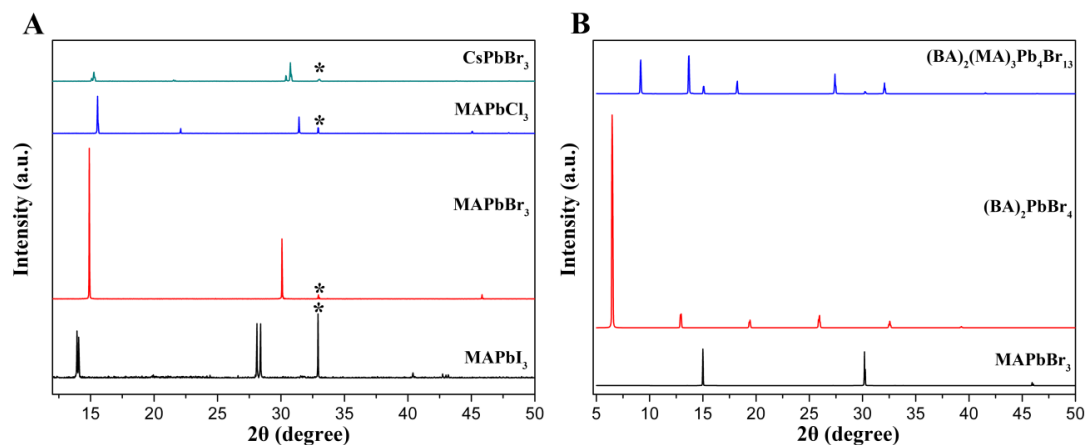


fig. S5. Powder XRD patterns of the perovskite single-crystal films. (A) Powder X-ray diffraction pattern of CsPbBr₃, MAPbCl₃, MAPbBr₃, MAPbI₃. (B) Powder X-ray diffraction pattern of MAPbBr₃, (BA)₂PbBr₄, and (BA)₂(MA)₃Pb₄Br₁₃. The peaks associated with silicon substrates are marked with asterisks.

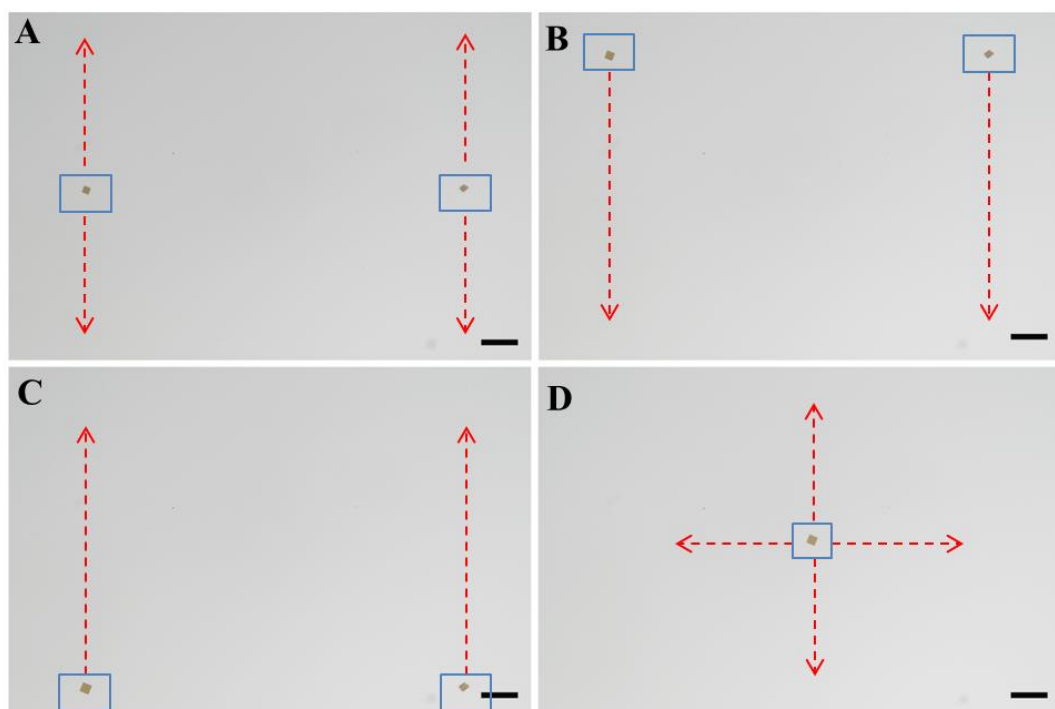


fig. S6. Optical microscopy images of the seed crystal regions. (A-D) Optical microscopy images of the certain arbitrary two seed crystals with the distance one millimeter after growing 30 minutes, by moving the microscope stage. It shows that no excrescent nucleation was founded around the seed crystals within 1 mm. The random nucleation can be effectively suppressed around the seed crystals within 1 mm. The scale bar is 0.1 mm.

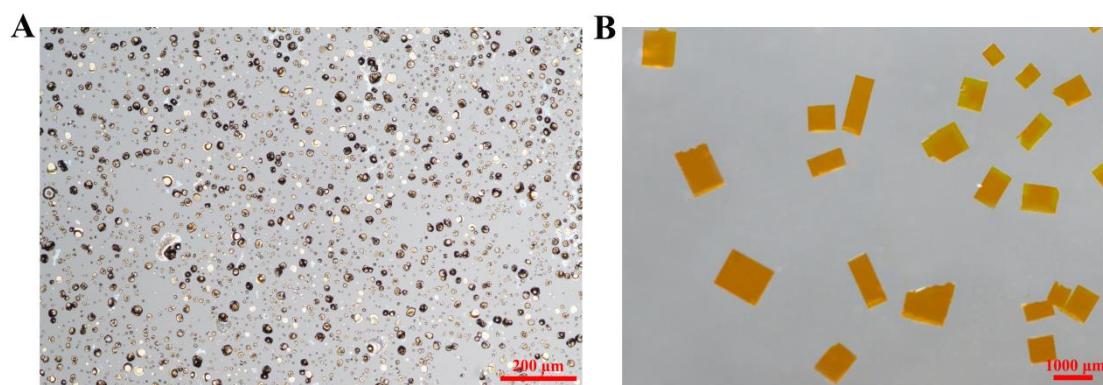


fig. S7. Scalable fabrication of perovskite single-crystal films. Optical microscopy images of the crystallization result of the random nucleation method (A) and (B) the crystallization system with introduced seed crystals. The random nucleation was effectively inhibited resulting in controllable growth of perovskite single-crystal films in batches.

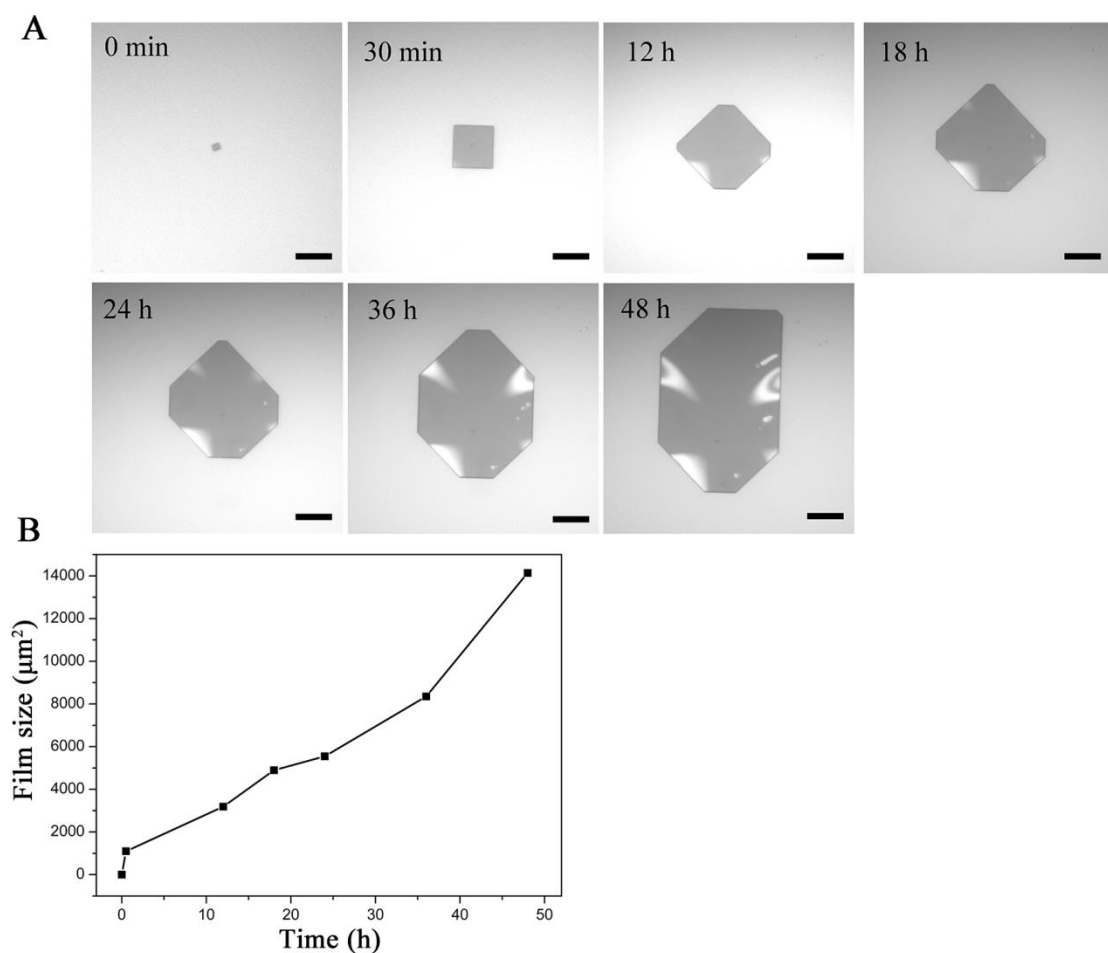


fig. S8. Perovskite single-crystal film growth process. (A) Optical microscopy images of the time-dependent seed growth in 48 hours. The scale bar is 30 μm . (B) The film size as a function of the growing time.

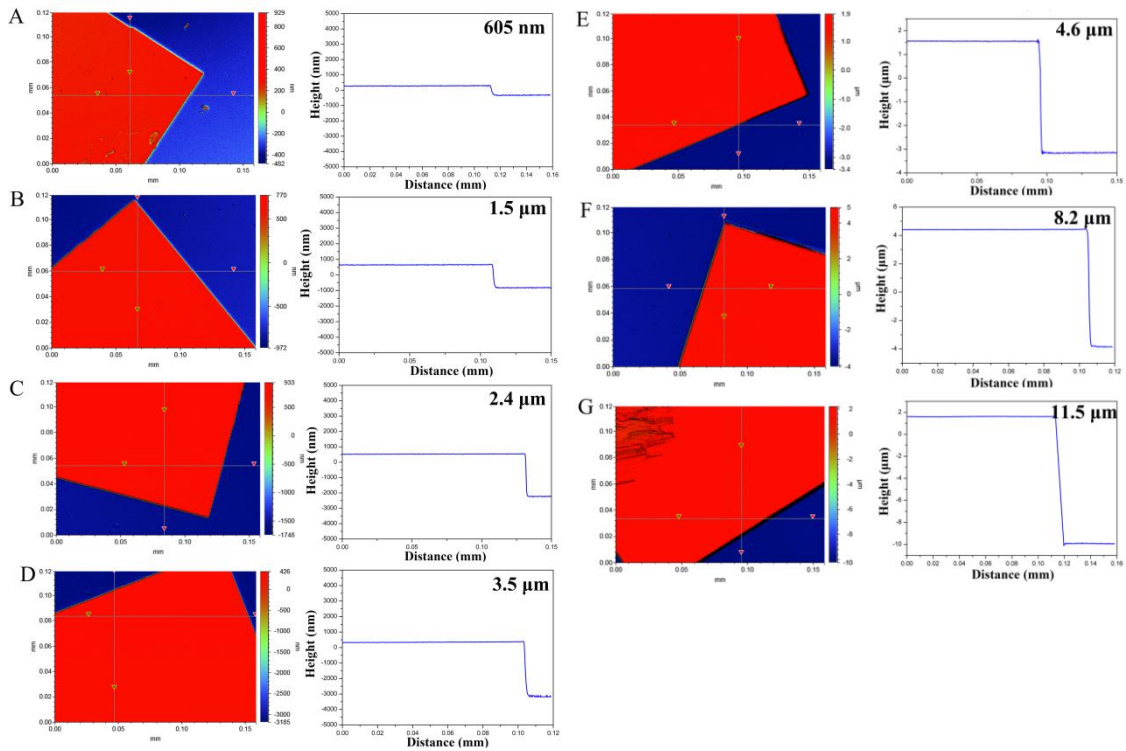


fig. S9. The height profiles of perovskite single-crystal films with different thicknesses. (A) 605 nm, (B) 1.5 μm , (C) 2.4 μm , (D) 3.5 μm , (E) 4.6 μm , (F) 8.2 μm , (G) 11.5 μm .

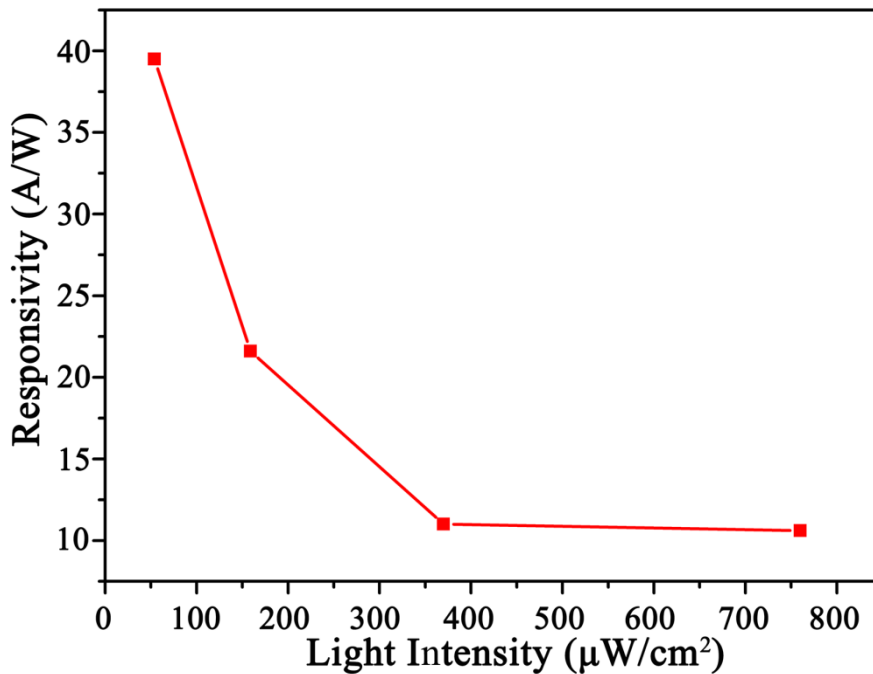


fig. S10. Responsivity as a function of incident light intensity. The measurement was performed at 5 V and a 450 nm laser source.